J. Fluid Mech. (2002), *vol.* 463, *pp.* 201–227.
DOI: 10.1017/S0022112002008728 Printed in the United Kingdom

Suboptimal feedback control of turbulent flow over a backward-facing step

By SEONGWON KANG AND HAECHEON CHOI†
School of Mechanical and Aerospace Engineering, Seoul National University, Seoul 151-742, Korea

(Received 13 June 2000 and in revised form 12 November 2001)

The objective of the present numerical study is to increase mixing in turbulent flow behind a backward-facing step using a systematic feedback control method. Spatially and temporally varying blowing and suction with zero-net mass flow rate are provided at the step edge, based on the sensing of the spanwise distribution of the wall pressure fluctuations at a downstream location. The cost functional to be increased is the root-mean-square spanwise pressure-gradient fluctuations at the sensing location, which may be associated with mixing behind the backward-facing step. Given the cost functional, the actuation at the step edge is determined through the suboptimal feedback control procedure of Choi *et al.* (1993). Large-eddy simulations of turbulent flow are conducted at a Reynolds number of 5100 based on the step height and free-stream velocity. The results of suboptimal feedback controls are compared with those of non-feedback single-frequency actuations. In case of the suboptimal control, velocity and vorticity fluctuations substantially increase downstream of the backward-facing step as well as in the recirculation zone. As a result, the reattachment length is significantly reduced, as compared to those of uncontrolled flow and flow with single-frequency actuations. A simple open-loop control method is devised from the suboptimal feedback control result, producing nearly the same mixing enhancement as the feedback control.

1. Introduction

Turbulent flow over a backward-facing step shows various phenomena such as separation, mixing-layer evolution, reattachment and redeveloping to turbulent boundary layer, as noted by previous workers (e.g. Eaton & Johnston 1981). Owing to its complexity, the flow has been considered as one of the most important problems in testing turbulence models. Therefore, many experimental and numerical studies have been conducted so far.

Recently, workers have been interested in this flow for the purpose of control, such as mixing enhancement behind the backward-facing step. Although the mixing efficiency may be measured from the probability density function of the mixture fraction of a passive scalar (Pumir 1994; Karasso & Mungal 1997), simpler expressions for mixing have often been used such as the r.m.s. (root-mean-square) velocity or vorticity fluctuations, reattachment length, etc. Among them, the reattachment length has been considered as one of the indices in representing mixing behind the backward-facing step (see below).

† Author to whom correspondence should be addressed: e-mail: choi@socrates.snu.ac.kr. Also at the National CRI Center for Turbulence and Flow Control Research, Institute of Advanced Machinery and Design, Seoul National University.

There have been many active and passive controls for turbulent flow over a backward-facing step; for example, uniform mass bleed (Yang, Tsai & Tsai 1994), upstream cavity or rod (Isomoto & Honami 1989), periodic blowing and suction at the edge (see below), surface rib or groove (Selby, Lin & Howard 1990; Kim & Chung 1995), porous wall (Heenan & Morrison 1998) and small particles (Fessler & Eaton 1999). Among them, the periodic blowing and suction (i.e. at a specific frequency) at the backward-facing step edge is an attractive control input because there is no net mass flow rate provided into the flow field. Numerous studies have been performed in this direction (e.g. Bhattacharjee, Scheelke & Troutt 1986; Roos & Kegelman 1986; Hasan & Khan 1992; Chun & Sung 1996; Chun, Lee & Sung 1999). In general, it has been found that the growth of roll-up vortices and their interactions such as pairing are enhanced at a certain range of actuation frequencies and the reattachment length is reduced. Sigurdson (1995) gives a succinct review on the periodic forcing in various geometries.

Separated flow behind a backward-facing step has a close similarity to a plane mixing layer. Work on plane mixing layers has shown that the behaviour of mixing-layer evolution depends significantly on the flow status of the incoming boundary layer. When the incoming flow is laminar, the flow downstream depends strongly on incoming flow conditions (Lasheras, Cho & Maxworthy 1986). The most commonly observed flow structures in this flow are the primary roll-up vortices and the secondary streamwise vortices. These streamwise rib vortices together with pairing of roll-up vortices play an important role of increasing entrainment (Lasheras *et al.* 1986; Bell & Mehta 1990, 1993). When incoming flow is turbulent, however, the streamwise rib vortices still exist in the flow (Breidenthal 1981; Bernal & Roshko 1986), but no steady pattern is observed (Bell & Mehta 1990). They make a considerable contribution to entrainment, but lower growth rate than in the laminar counterpart is attributed to the absence of the organized (steady) streamwise vortical structures in turbulent flow (Bell & Mehta 1990).

The connection between the streamwise rib vortices and entrainment has attracted workers to use this concept for mixing control. Nygaard & Glezer (1994) and Collis *et al.* (1994) imposed time-harmonic excitations having spanwise-non-uniform phase or frequency distributions on developing mixing layers. They observed mixing enhancement and the 'chain-link-fence' vortical structure which is different from the usual rib/roller vortex found in a plane mixing layer. Bell & Mehta (1993) generated spanwise perturbations upstream of a mixing layer, to investigate how the imposed organized streamwise vortices change the entrainment process in a turbulent mixing layer. They observed an entrainment increase in the near-field region, but a decrease in the far-field region, because the imposed streamwise vortices disturbed the standard pairing process.

Work conducted on mixing layers suggests that generating streamwise vortices at or before a backward-facing step may be a possible control strategy for increasing mixing in turbulent flow behind the step. The previous studies on this flow have paid primary attention to two-dimensional vortical interaction generated by uniform (in space) but periodic (in time) blowing and suction. In the present study, by providing spatially and temporally varying blowing and suction into the flow, we want to achieve larger mixing than the method based on two-dimensional vortical interaction. The blowing and suction will be given from a spanwise slot located at the backward-facing step edge. We know of only one previous study where spatially and temporally varying blowing and suction are applied to this flow; Chun *et al.* (1999) applied spanwise-varying (via a banded thin tape covering the blowing/suction slot) and

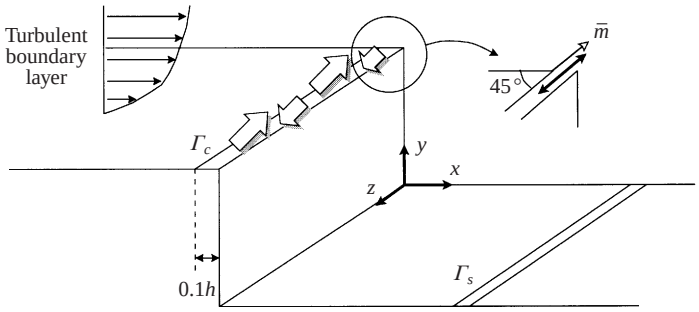

FIGURE 1. Schematic diagram of the feedback control.

time-varying (with single-frequency forcing) blowing and suction to turbulent flow over a backward-facing step, and showed that the reattachment length can be further reduced when a proper combination of open and blocked slot areas is found, but the amount of reduction (or the amount of mixing enhancement) is not substantial even in the optimal case. In our study, the blowing and suction, which vary in the spanwise direction and time, are determined by the suboptimal feedback control procedure which was originally developed by Choi *et al.* (1993) and further developed and applied to other flow fields by Bewley *et al.* (1993), Satake & Kasagi (1997), Lee, Kim & Choi (1998) and Min & Choi (1999). Similar optimal or suboptimal control procedures have been applied to laminar flow over a backward-facing step (Choi, Hinze & Kunisch 1999; Hou & Ravindran 1998, 1999), but there is no previous study in which a feedback control method based on a mathematical control theory is applied to turbulent flow over a backward-facing step.

The objective of the present study is to increase mixing in turbulent flow behind a backward-facing step by applying the suboptimal feedback control method. The incoming flow before the step is a turbulent boundary-layer flow and thus this work is associated with turbulent separation control. The turbulent flow field is generated using the large-eddy simulation (LES) technique. The actuation provided at the step edge is spatially and temporally varying blowing and suction with zero-net mass flow rate. The control procedure is presented in § 2, and the computational details are described in § 3. The results of non-feedback single-frequency actuations and suboptimal feedback control are presented and compared in § 4. An open-loop control method obtained from the result of the suboptimal feedback control is also presented in § 4, followed by summary and concluding remarks in § 5.

2. Control method

2.1. *Problem setting*

As stated in § 1, we provide a feedback actuation (blowing and suction) from a spanwise slot installed at the step edge Γ_c (figure 1), to increase mixing behind the backward-facing step. The actuation slot is located at $-0.1h \leqslant x \leqslant 0$ and $y = h$, where h is the step height. The angle of actuation is 45° with respect to the streamwise direction. This configuration is determined by considering previous experimental conditions and the computational aspect. The actuation varies in the spanwise direction and time, based on sensing at Γ_s. We will later develop an open-loop control method of increasing mixing from the result of the feedback control (§ 4).

As a sensing variable for feedback, we choose the pressure fluctuation on the downstream wall, because the pressure is a global quantity and obviously has some effect on the way the control algorithm works. For instance, the r.m.s. wall-pressure fluctuations peak at about $1h$ upstream of the mean reattachment position (see, for example, Eaton & Johnston 1981) because the wall-pressure fluctuations are generated primarily by the large eddies which reattach. Moreover, it was shown in Eaton & Johnston (1980) that low-frequency (i.e. large time scale) oscillations in these types of flow make a significant contribution to the wall-pressure fluctuations. Therefore, in the present study, the pressure fluctuation is selected as a sensing variable for feedback, and the position at which it is sensed is chosen to be near the reattachment location. On the other hand, the r.m.s. wall-pressure fluctuations can be sufficiently large even in the case of two-dimensional unsteady flow, but in this case there is no mixing in the third direction. In order to avoid this situation, we finally select the sensing variable as the wall pressure-gradient fluctuation in the spanwise direction, which is also related to the streamwise-vorticity flux at the wall.

Therefore, we define the cost functional to be increased owing to the actuation at Γ_c as:

$$J(\phi) = \frac{1}{2}\int_{\Gamma_s}\left(\frac{\partial p'}{\partial z}\right)^2 \mathrm{d}z\,\mathrm{d}x, \tag{2.1}$$

where p' is the pressure fluctuation, ϕ is the actuation provided at Γ_c, and Γ_s is the sensing location near the reattachment position. The actuation values at Γ_c of increasing J are determined from the suboptimal feedback control procedure based on the sensing of p' at Γ_s. The detailed procedure is shown in the next section.

2.2. *Suboptimal feedback control procedure*

The governing equations for fluid flow and the boundary conditions for the present problem are, respectively,

$$\frac{\partial u_i}{\partial t} + \frac{\partial u_i u_j}{\partial x_j} = -\frac{\partial p}{\partial x_i} + \frac{1}{Re}\frac{\partial^2 u_i}{\partial x_j \partial x_j}, \tag{2.2}$$

$$\frac{\partial u_i}{\partial x_i} = 0, \tag{2.3}$$

and

$$\left.\begin{array}{ll} u_i = \phi(z) m_i & \text{on } \Gamma_c, \\ u_i = \text{given} & \text{elsewhere,} \end{array}\right\} \tag{2.4}$$

where t is the time, $Re = U_0 h/\nu$ is the Reynolds number, U_0 is the free-stream velocity, h is the step height, ν is the kinematic viscosity, and m_i is the unit vector along the direction of blowing (see figure 1). The boundary conditions are described in detail in § 3.2.

Let us consider the suboptimal control procedure as proposed in Choi *et al.* (1993), in which we aim at practical implementation of feedback control at the expense of losing the predictability of the control effect in a large time interval:

(i) discretize the governing equation in time;

(ii) at each instance of time, we are directing the flow in a direction that produces an increase in the instantaneous cost functional (2.1).

Therefore, for the first step, we choose the Crank–Nicolson scheme for the pressure gradient and viscous diffusion terms and the Adams–Bashforth scheme for the

convection terms to yield a discretized system of (2.2)–(2.4):

$$u_i^{n+1} + \frac{\Delta t_c}{2}\frac{\partial p^{n+1}}{\partial x_i} - \frac{\Delta t_c}{2Re}\frac{\partial^2 u_i^{n+1}}{\partial x_j \partial x_j} = RHS_i^n, \tag{2.5}$$

$$\frac{\partial u_i^{n+1}}{\partial x_i} = 0, \tag{2.6}$$

with

$$\left.\begin{aligned} u_i^{n+1} &= \phi^{n+1}(z) m_i \quad \text{on } \Gamma_c, \\ u_i^{n+1} &= \text{given} \qquad\quad \text{elsewhere,} \end{aligned}\right\} \tag{2.7}$$

where Δt_c is the control time interval (i.e. the time interval between the consecutive control updates, which is not necessarily the computational time step used for integrating the governing equation in time), and the superscript $n+1$ denotes the control time step at which a new actuation is applied. RHS_i^n contains the convection terms and the explicit parts of the pressure gradient and viscous diffusion terms at the control time step n.

As mentioned in § 2.1, the cost functional J is a function of the actuation ϕ and we must find the sensitivity of J with respect to ϕ to increase the cost functional (2.1). In order to determine the sensitivity, we introduce the Fréchet differential states of the velocity and pressure (q_i, ρ) using the Fréchet differential (Finlayson 1972):

$$q_i = \frac{\mathscr{D} u_i^{n+1}}{\mathscr{D}\phi^{n+1}}\tilde{\phi}^{n+1}, \tag{2.8}$$

$$\rho = \frac{\mathscr{D} p^{n+1}}{\mathscr{D}\phi^{n+1}}\tilde{\phi}^{n+1}, \tag{2.9}$$

with

$$\frac{\mathscr{D} f^{n+1}(\phi)}{\mathscr{D}\phi^{n+1}}\tilde{\phi}^{n+1} = \lim_{\epsilon \to 0}\frac{f^{n+1}(\phi + \epsilon\tilde{\phi}) - f^{n+1}(\phi)}{\epsilon}, \tag{2.10}$$

where $\tilde{\phi}$ is an arbitrary perturbation to ϕ. The Fréchet differential is applied to (2.5)–(2.7), which yields the following governing equations for (q_i, ρ) and boundary conditions:

$$q_i + \frac{\Delta t_c}{2}\frac{\partial \rho}{\partial x_i} - \frac{\Delta t_c}{2Re}\frac{\partial^2 q_i}{\partial x_j \partial x_j} = 0, \tag{2.11}$$

$$\frac{\partial q_i}{\partial x_i} = 0, \tag{2.12}$$

with

$$\left.\begin{aligned} q_i &= \tilde{\phi}(z) m_i \quad \text{on } \Gamma_c, \\ q_i &= 0 \qquad\quad \text{elsewhere.} \end{aligned}\right\} \tag{2.13}$$

Note that RHS_i^n in (2.5) disappears in (2.11) because there is no effect of ϕ^{n+1} on the past flow fields. The boundary conditions for q_i are zero only when they are not influenced by the actuation ϕ^{n+1}. Therefore, there may be non-zero boundary conditions for q_i at the outflow and far-field boundaries. However, numerical tests for the effect of actuation on the boundary conditions have shown in this study that the effect is negligible when the outflow and far-field boundaries are located sufficiently far away from the actuator.

It is clear from the above that the choice of the time-discretization scheme strongly

affects (2.11) and thus the result of the suboptimal control may change significantly depending on the time-discretization scheme. For example, applying an explicit scheme such as the Adams–Bashforth scheme to the convection terms results in no contribution from the convection terms to (2.11). Thus, the control algorithm may miss an important fluid dynamics effect. However, Lee *et al.* (1998) found from numerical tests with the convection terms included in (2.11) that the contribution from the convection terms is negligible in a short time interval Δt_c in the boundary control of turbulent channel flow. In the present study, we also included the convection terms in (2.11) by applying the Crank–Nicolson scheme, reaching the same conclusion as in Lee *et al.* (1998). In the present flow configuration, the actuation at the edge of the backward-facing step instantaneously affects the flow at the sensor location (near the reattachment position) through the pressure, whereas it takes a much longer time to affect the flow through the convection because of the distance between the sensor and actuator. Therefore, including the convection terms in (2.11) does not change the actuation in a short time interval Δt_c. (It is also noted that including the convection terms in (2.11) may not be practical in real implementation, because it requires the sensing of the velocity inside the flow domain (Choi *et al.* 1993).) In order to include the effect of the convection, we may have to employ an optimal control procedure (Abergel & Temam 1990; Bewley & Moin 1999), where the cost functional is defined on a large time interval. In this case, however, the iterative solutions of the Navier–Stokes equations and the corresponding control (adjoint) equations are required on the large time interval together with flow-variable sensing in the whole flow field.

The Fréchet differential system (2.11)–(2.13) can be solved analytically with the aid of the Fourier transform in a simple geometry where the technique of separation of variables is applied (Lee *et al.* 1998; Min & Choi 1999). However, when the flow geometry is complex, it is not, in general, possible to solve (2.11)–(2.13) analytically owing to the arbitrary boundary condition $\tilde{\phi}(z)$. In this case, we may solve the adjoint Navier–Stokes equations numerically with proper adjoint boundary conditions, which are derived from the Fréchet differential equations and the cost functional (Choi *et al.* 1993). However, the adjoint system should be solved at every control time step, which imposes an additional computational load. In the present study, an approach using the linear characteristic of the Fréchet differential system (2.11)–(2.13) is considered.

Let us define a system of (η_i, π) as follows:

$$\eta_i + \frac{\Delta t_c}{2}\frac{\partial \pi}{\partial x_i} - \frac{\Delta t_c}{2Re}\frac{\partial^2 \eta_i}{\partial x_j \partial x_j} = 0, \tag{2.14}$$

$$\frac{\partial \eta_i}{\partial x_i} = 0, \tag{2.15}$$

with

$$\left.\begin{aligned} \eta_i &= \delta(z) m_i \quad \text{on } \Gamma_c, \\ \eta_i &= 0 \qquad\quad \text{elsewhere,} \end{aligned}\right\} \tag{2.16}$$

where $\delta(z)$ denotes the Dirac delta function. Then the solution (q_i, ρ) of (2.11)–(2.13) is given as the following convolution integral form:

$$\left.\begin{aligned} q_i(x, y, z) &= \int_0^{L_z} \eta_i(x, y, z-\zeta)\tilde{\phi}(\zeta)\,\mathrm{d}\zeta, \\ \rho(x, y, z) &= \int_0^{L_z} \pi(x, y, z-\zeta)\tilde{\phi}(\zeta)\,\mathrm{d}\zeta, \end{aligned}\right\} \tag{2.17}$$

where L_z is the spanwise length of Γ_c.

By taking the Fréchet derivative of the cost functional (2.1) and using (2.17), we can easily obtain the sensitivity of J with respect to ϕ,

$$\frac{\mathscr{D}J(z)}{\mathscr{D}\phi} = \int_{\Gamma_s} \frac{\partial p'(\zeta)}{\partial \zeta} \frac{\partial \pi'(\zeta - z)}{\partial \zeta} \, \mathrm{d}\zeta \, \mathrm{d}x. \tag{2.18}$$

The actuation value ϕ^{n+1} of increasing the cost functional J is obtained using a gradient algorithm

$$\phi^{n+1^{k+1}} - \phi^{n+1^k} = \varrho \frac{\mathscr{D}J\left(\phi^{n+1^k}\right)}{\mathscr{D}\phi^{n+1}}, \tag{2.19}$$

where k denotes the iteration index, and ϱ is the ascent parameter which has a positive value. Then, the cost functional J increases with k:

$$J(\phi^{n+1^{k+1}}) \approx J(\phi^{n+1^k}) + \frac{\mathscr{D}J(\phi^{n+1^k})}{\mathscr{D}\phi^{n+1}} (\phi^{n+1^{k+1}} - \phi^{n+1^k}), \tag{2.20}$$

$$J(\phi^{n+1^{k+1}}) \approx J(\phi^{n+1^k}) + \varrho \left| \frac{\mathscr{D}J(\phi^{n+1^k})}{\mathscr{D}\phi^{n+1}} \right|^2. \tag{2.21}$$

We should iterate (2.19) to obtain an optimal actuation value. Although it does not pose any difficulties in a purely computational study, the iterative approach is not practical because no iteration is allowed in real implementation, i.e. in an experiment, in order to obtain an optimal actuation value, we have to iteratively measure the change of the wall pressure (p^{n+1^k} at Γ_s) due to ϕ^{n+1^k} at a fixed u_i^n, which is impossible in practice. Thus only one-time evaluation of $\mathscr{D}J/\mathscr{D}\phi$ is allowed for practical implementation. In this case, we cannot guarantee the maximum J. The effect of the number of iterations on the control output is studied in Choi *et al.* (1993). Recently, Choi *et al.* (1999) used a line search to find a proper value of the ascent parameter ϱ, which is still impractical because one additional iteration is required in that approach. Therefore, in the present study, the actuation at each control time step is decided as follows:

$$\phi^{n+1}(z) = \varrho \int_{\Gamma_s} \frac{\partial p'(\zeta)}{\partial \zeta} \frac{\partial \pi'(\zeta - z)}{\partial \zeta} \, \mathrm{d}\zeta \, \mathrm{d}x. \tag{2.22}$$

As shown in this section, our approach avoids solving the adjoint equations and finds the solution of Fréchet differential equations in terms of the convolution integral. We solve the system (2.14)–(2.16) numerically and store the solution π. Then we obtain ϕ through the convolution integral (2.22) with the measurement of p' at Γ_s at every control time step. In the present study, ϱ is determined such that the r.m.s. of $\phi(z)$ is constant in time through the computation. Our approach shown in this section, i.e. solving (2.14)–(2.15) with the Dirac delta function defined at $z = 0$ and obtaining the blowing and suction from the convolution integral (2.22), is still limited to certain flow geometries in that it is only applicable to a periodic or infinite domain. For other flow geometries, solving the adjoint Navier–Stokes equations with proper adjoint boundary conditions may be more convenient for determining the actuation.

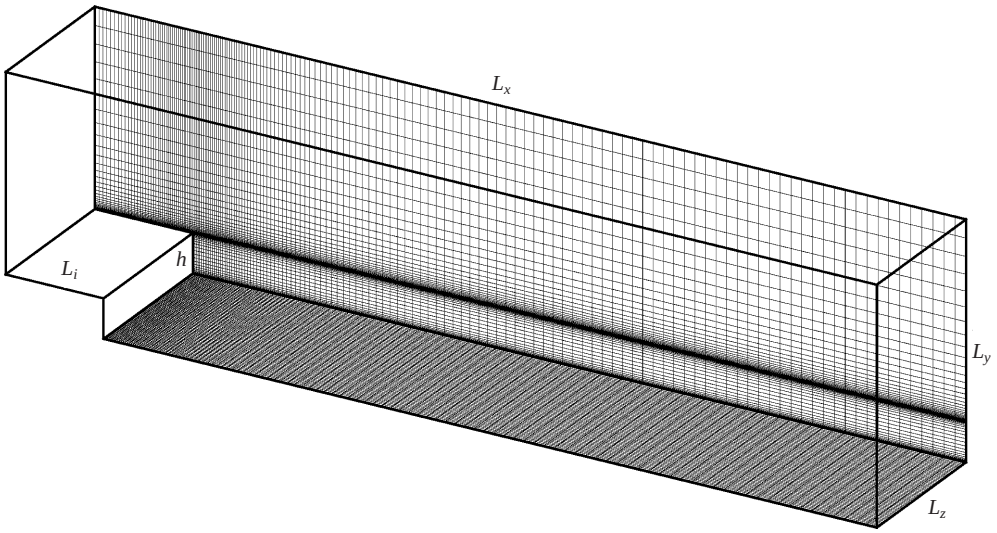

FIGURE 2. Computational domain and grid system.

3. Computational details

3.1. *Computational domain and grid spacing*

Figure 2 shows the schematic diagram of the computational domain and grid system, where ($x = 0$, $y = h$) is the location of the backward-facing step edge. The computational domain size in each direction is $L_i = 2.5h$, $L_x = 22.5h$, $L_y = 6h$ and $L_z = 4h$, respectively, which is very similar to that used in Le, Moin & Kim (1997). The Reynolds number based on the free-stream velocity U_0 and step height h is 5100 and the Reynolds number based on the free-stream velocity and displacement thickness δ^* at $x = -2.5h$ is 1058.

Non-uniform grid distributions are used in both the streamwise and wall-normal directions, and uniform grid distribution in the spanwise direction. Grids are clustered near the step edge and bottom wall using tangent hyperbolic functions. The number of grid points used is $151 \times 56 \times 64$ in the streamwise, wall-normal and spanwise directions, respectively. In the wall-normal direction, 32 grids are used at $y \geqslant h$, and 38 grids are used in the streamwise direction at the inlet section before the step ($x \leqslant 0$). The total number of grid points used here is about twice that used in Akselvoll & Moin (1995).

3.2. *Numerical scheme and boundary conditions*

The governing equations for unsteady incompressible viscous flow and boundary conditions for the present problem are shown in (2.2)–(2.4). The numerical scheme to solve (2.2)–(2.3) is essentially the same as that used by Akselvoll & Moin (1995). That is, a variant of the fractional step method (Kim & Moin 1985) is employed to treat implicit coupling of the Navier–Stokes and continuity equations. The Crank–Nicolson method is used for the convection and diffusion terms in the wall-normal direction, and a third-order Runge–Kutta scheme is used for all the other terms. The nonlinear equation resulting from the implicit treatment of the convection term is linearized without losing the second-order time accuracy (see Akselvoll & Moin 1995). The second-order central difference is used for all the terms in a staggered grid system. The LES technique is used with a dynamic subgrid-scale model (Germano *et al.* 1991;

Lilly 1992). For the suboptimal feedback control, (2.14)–(2.16) are solved using the preconditioned conjugate gradient method by Glowinski & Pironneau (1992).

The no-slip condition is used at the wall, and the periodic boundary condition is used in the spanwise direction. At $y = L_y$, the following no-stress condition is used assuming symmetry at the upper boundary (Le *et al.* 1997):

$$\frac{\partial u}{\partial y} = 0, \quad v = 0, \quad \frac{\partial w}{\partial y} = 0. \tag{3.1}$$

The blowing/suction slot is located at $-0.1h \leqslant x \leqslant 0$ and $y = h$. The angle of actuation is 45° with respect to the streamwise direction (see figure 1). The blowing/suction profile at the slot is determined by (2.22) in case of the suboptimal feedback control.

For the present computation, a separate LES of turbulent boundary-layer flow is performed to provide realistic inlet turbulence at $x = -2.5h$ based on the method by Lund, Wu & Squires (1998). In Lund *et al.*, the inlet turbulence is generated through a sequence of operations where the velocity field at a downstream (recycling) location is rescaled using empirical scaling laws and re-introduced at the inlet. This method is shown to produce a realistic turbulent boundary layer with accurate velocity statistics. In our separate LES of turbulent boundary-layer flow, the recycling location is placed $50\delta^*_{in}$ downstream of the inlet, corresponding to $10.4h$, where δ^*_{in} is the inlet displacement thickness. Therefore, we may wonder if the recycling of the velocity data at a downstream location imposes a feedback forcing at a frequency of about $0.1U_0/h$ (assuming that the convection velocity of turbulence structures is about U_0), which may considerably affect the reattachment behind the backward-facing step. However, the velocity spectra obtained through the recycling procedure do not show any distinctive peaks near this frequency. The inflow data are stored in advance and provided in time at the inlet of flow over the backward-facing step. The actuation provided at the slot ($x = 0$) disturbs the upstream flow only up to $x = -h$. Therefore, the inflow data provided at $x = -2.5h$ should be adequate for the present study.

The boundary condition at the exit is the convective outflow condition (Pauley, Moin & Reynolds 1990),

$$\frac{\partial u_i}{\partial t} + U_c \frac{\partial u_i}{\partial x} = 0, \tag{3.2}$$

where U_c is the convection velocity which is the plane-averaged streamwise velocity at the exit. This boundary condition allows vortices to pass away smoothly from the computational domain.

For the special selection of the time advancement scheme considered in this study, the CFL number for the computational time step limit is defined as

$$CF_c = \left|\frac{u\Delta t}{\Delta x}\right| + \left|\frac{w\Delta t}{\Delta z}\right| + \frac{4\Delta t}{Re\Delta x^2} + \frac{4\Delta t}{Re\Delta z^2}. \tag{3.3}$$

For the simulation of the backward-facing step flow without control, we used $\Delta t = 0.015h/U_0$ ($CF_c \approx 0.5$) which is smaller than $0.02h/U_0$ selected by Akselvoll & Moin (1995). The simulation had been run for a total of $1050h/U_0$. Initial flow fields for $750h/U_0$ were discarded and the flow fields were averaged for the remaining $300h/U_0$. For all the control cases considered here, the same Δt ($= 0.015h/U_0$) was used during the simulation. The flow fields were averaged for $150h/U_0$ after a transient time of $112.5h/U_0$. The CPU time required was about 3 Cray YMP C90 seconds per time step.

4. Results

4.1. *Uncontrolled case*

In this section, the result from the LES of turbulent flow over the backward-facing step without control is presented and compared with those of the previous DNS (Le *et al.* 1997) and LES (Akselvoll & Moin 1995). The Reynolds number is 5100 based on U_0 and h. The boundary-layer thickness is $1.34h$ at $x = -2.5h$ and the Reynolds number based on δ^* at this position is 1058. Overall conditions are kept nearly the same as those in Le *et al.*

Figure 3 shows profiles of the mean streamwise velocity and r.m.s. streamwise velocity fluctuations at several streamwise locations, together with those of Le *et al.* (1997) and Akselvoll & Moin (1995). An excellent agreement is found among the data. The reattachment length (X_r) is $6.2h$ in the present study, which is slightly different from the previous DNS ($6.28h$) and LES ($6.35h$) results. The friction coefficient on the downstream wall without control is shown in figure 4, together with those of the previous DNS (Le *et al.* 1997) and experiment (Jovic & Driver 1994). The minimum C_f is -0.0037 in the present study which is lower than -0.0029 from DNS by Le *et al.* but closer to -0.0034 from the experiment by Jovic & Driver. The LES by Akselvoll & Moin produced nearly the same C_f curve as that of DNS. The discrepancy between the present and other simulation results is mainly due to the difference in the inflow generation technique. As stated before, we employed the recycling technique of Lund *et al.* (1998), whereas the previous DNS and LES used the phase jittering technique of Lee, Lele & Moin (1992). It is known that the latter technique requires a much longer transient distance to obtain fully developed turbulent boundary-layer flow than the former. Therefore, the inflow boundary conditions may not be exactly the same among three simulations, which can be found from the u_{rms} profiles at $y > h$ and $x = h$ in figure 3(b).

4.2. *Single-frequency actuations (SFA)*

Prior to the suboptimal feedback control, actuations at a single frequency (SFA) are applied to the current flow field. Controls using SFA have been studied by many workers in various geometries and have proved to be very effective in controlling flows (see § 1). Therefore, the control results from SFA will be compared with those obtained from the suboptimal control in § 4.3.

The blowing/suction value for SFA changes in time such that

$$\phi(t) = A_0 \sin[2\pi St_h t], \tag{4.1}$$

where A_0 is the amplitude and $St_h = fh/U_0$ is the Strouhal number (non-dimensional actuation frequency). A_0 is not exactly described in experiments and is thus set to be $0.1U_0$ in the present study. In SFA, there exists a specific range of frequency that minimizes the reattachment length, or maximizes mixing behind the step. In the present study, four cases of $St_h = 0.1$, 0.2, 0.3 and 0.4 are considered. Note that the input-power requirements are the same for all the cases. The reattachment lengths from four control cases are given in table 1. The maximum reduction of X_r by $1.2h$ (19.4%) occurs at $St_h = 0.2$. Experimental studies have also shown maximum reduction of X_r near $St_h = 0.2$ (Roos & Kegelman 1986; Chun & Sung 1996). The detailed features of the variations of the turbulence intensities, Reynolds shear stress, and vortical structures with respect to the actuation frequency have been carefully studied; however, these aspects are not the primary concern of this paper and thus will be reported elsewhere. Some of the statistics at $St_h = 0.2$ are compared with those obtained from the suboptimal control in the following section.

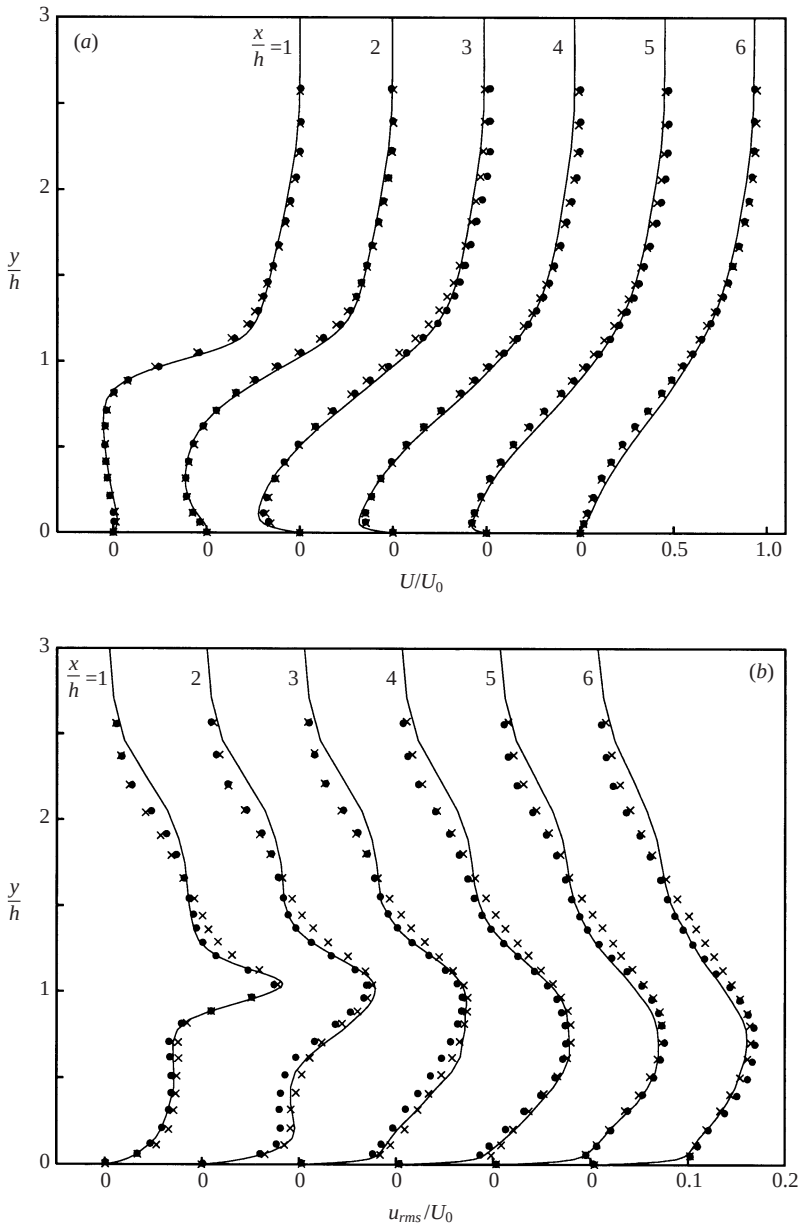

FIGURE 3. Profiles of the mean streamwise velocity and r.m.s. streamwise velocity fluctuations: ——, present study; •, DNS by Le *et al.* (1997); ×, LES by Akselvoll & Moin (1995). (*a*) U. (*b*) u_{rms}.

		St_h			
Case	Uncontrolled	0.1	0.2	0.3	0.4
X_r/h	6.2	5.5 (88.7%)	5.0 (80.6%)	5.4 (87.1%)	5.7 (91.9%)

TABLE 1. Variation of the reattachment length with respect to the actuation frequency. The values in the parentheses denote the percentages of the reattachment length to that of uncontrolled flow.

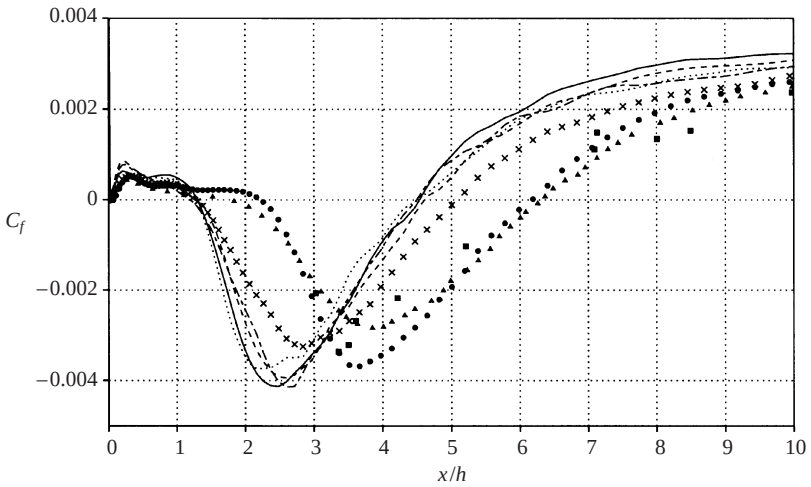

FIGURE 4. Friction coefficients on the downstream wall: •, uncontrolled; ▲, DNS by Le *et al.* (1997); ■, experiment by Jovic & Driver (1994); ×, SFA ($St_h = 0.2$); ——, SOF ($x_s = 4h$); – – –, SOF ($x_s = 5h$); · · ·, SOF ($x_s = 6h$); — · —, SOF ($5.5h < x_s < 6.5h$).

4.3. *Suboptimal feedback controls (SOF)*

The suboptimal control procedure shown in § 2 is applied to turbulent flow over the backward-facing step and its result is compared with that of SFA at $St_h = 0.2$. For SFA, the actuation (blowing/suction) changes only in time, providing a periodic spanwise vorticity to the flow behind the backward-facing step. On the other hand, for the suboptimal feedback control (SOF), the actuation changes both in time and space (spanwise direction). Therefore, the streamwise vorticity ($\partial v/\partial z \neq 0$) as well as the spanwise vorticity is generated at the slot from the actuation, letting us expect more mixing with SOF. The mass flux of blowing/suction averaged in time and space is zero for both SFA and SOF cases, and the r.m.s. value for SOF is kept the same as that for SFA, i.e. $\phi_{rms} = (0.1/\sqrt{2})U_0$, by adjusting the ascent parameter in (2.22).

The present suboptimal control procedure requires sensing of the wall pressure fluctuation at Γ_s for feedback (see (2.22)). In the present study, we consider four different sensor locations on the downstream wall; $x_s = 4h$, $5h$, $6h$ and $5.5h < x_s < 6.5h$. Here, as mentioned in § 2.1, the sensors are placed near the mean reattachment position. The first three cases correspond to sensing on a line, whereas the fourth case to sensing on an area. The control time interval Δt_c is selected to be $\Delta t_c = 4\Delta t = 0.06h/U_0$. That is, the sensing and actuation are updated at every 4 computational time steps. Because the control time interval used in this study was much smaller than the time scale of large eddies, different Δt_c ($\Delta t_c = 0.12h/U_0$ or $0.03h/U_0$) changed the results only slightly as compared to those obtained from $\Delta t_c = 0.06h/U_0$. When the sensors are placed very near the actuators, however, numerical instability or undesirable control results may occur at $\Delta t_c = \Delta t$. For example, when the sensors and actuators are placed at the same location, the actuation generates $\partial v/\partial z$ (one component of the streamwise vorticity) at the wall, which is directly associated with the spanwise pressure gradient $\partial p'/\partial z$ (streamwise-vorticity flux) there. Therefore, in this case, the actuation itself changes the sensing variable at the sensor location (and thus the cost functional). Furthermore, at $\Delta t_c = \Delta t$, the actuation profile is determined by the sensing variable that is at the same time modified by the actuation itself. This process produces numerical instability or undesirable control results in a few time steps.

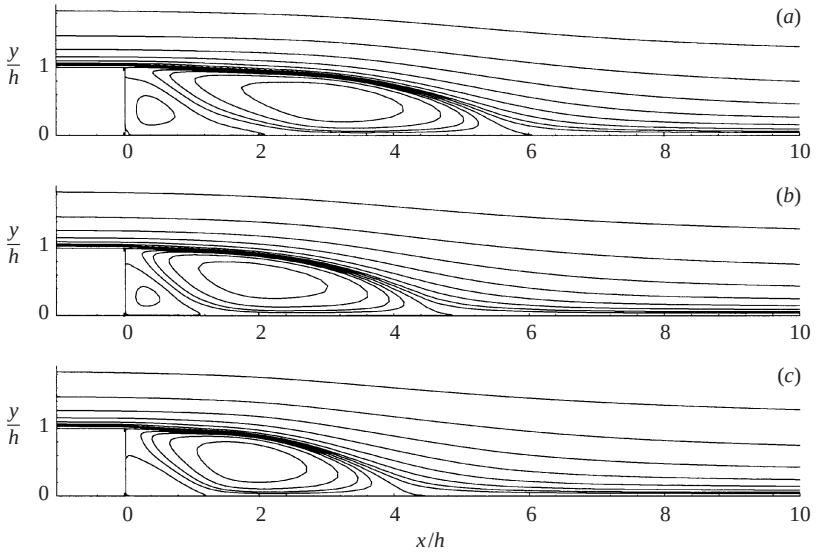

FIGURE 5. Time-averaged streamlines: (*a*) uncontrolled; (*b*) SFA ($St_h = 0.2$); (*c*) SOF ($x_s = 6h$). The contour levels are $-0.005 \times 2^m, 0, 0.005 \times 2^n$, where $m = 0, 1, 2, 3$ and $n = 0, 1, \ldots, 7$.

4.3.1. *Turbulence statistics*

The averaged flow fields from SOF are obtained and compared with those from the uncontrolled and SFA ($St_h = 0.2$) cases. As stated earlier, the objective of the present study is to increase mixing behind the backward-facing step and we consider the reattachment length as one of the performance indices. Figure 4 shows the friction-coefficient (C_f) profiles for the uncontrolled, SFA and SOF cases. The reattachment lengths for the SOF cases range from $4.4h$ to $4.6h$. Therefore, SOF reduces the reattachment length more by the amount of $0.4h \sim 0.6h$ (6.5% $\sim$ 9.7%) than SFA. Note that the effect of the sensor location on the reattachment length is shown to be only marginal once the location for the sensor is near the reattachment position, suggesting that the mechanism of the reattachment length reduction is essentially the same for all the cases. The region of positive C_f in the recirculating bubble becomes smaller with controls, indicating that a smaller secondary bubble exists near the corner of the backward-facing step.

Figure 5 shows the time-averaged streamlines for the uncontrolled, SFA and SOF cases. As was mentioned above, the recirculating bubble is smallest for SOF. The streamwise length of the secondary bubble for SOF is nearly the same as that for SFA, but is smaller than that for the uncontrolled case. The wall-normal (y) length of the secondary bubble is also smallest for SOF.

Figures 6(a) and 6(b) show the r.m.s. wall-normal and spanwise velocity fluctuations, respectively. It is seen that the r.m.s. cross-plane velocity fluctuations inside the recirculating bubble significantly increase owing to SOF, indicating mixing enhancement due to control. The increase is even more than that of SFA, especially in the spanwise velocity component, which is a natural consequence of the definition of our cost functional (pressure gradient fluctuations in the spanwise direction) and spanwise-varying actuations.

Figure 7 shows the variation of the maximum spanwise turbulence intensity along the streamwise direction owing to controls. The maximum spanwise turbulence in-

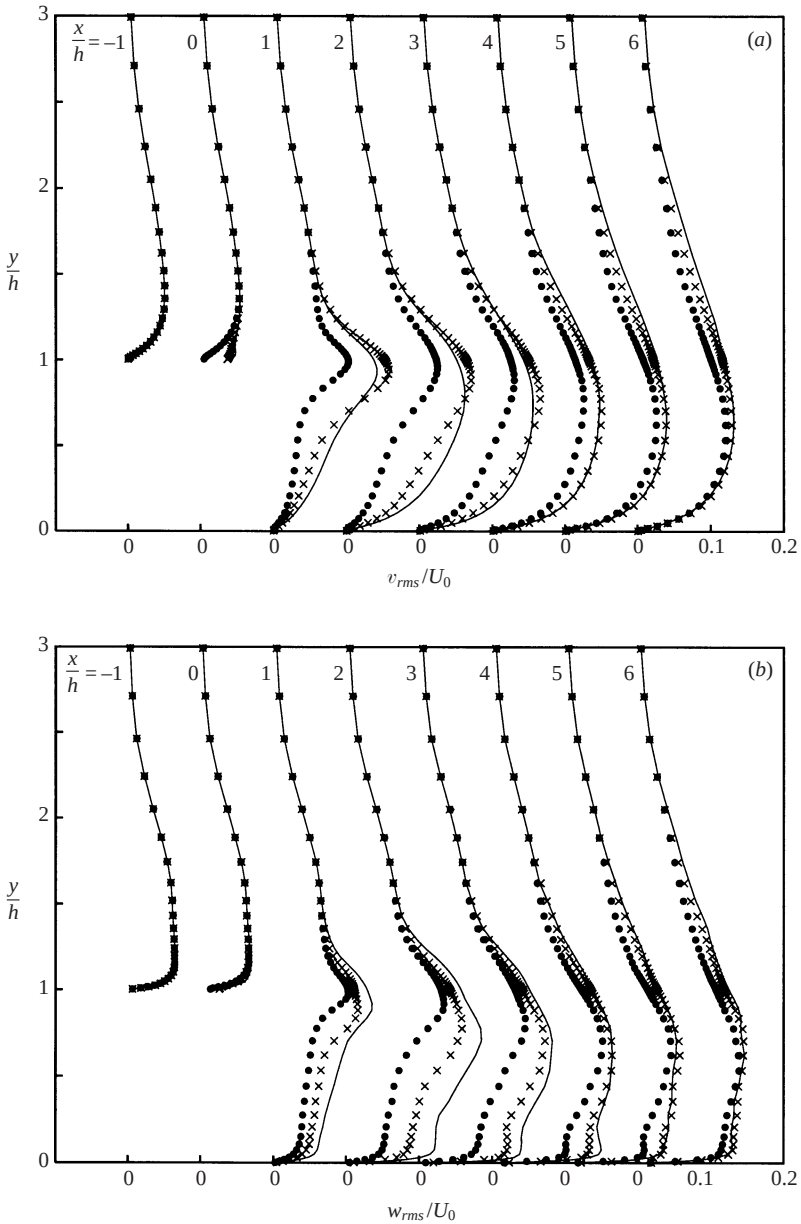

FIGURE 6. Root-mean-square velocity fluctuations: •, uncontrolled; ×, SFA ($St_h = 0.2$); ——, SOF ($x_s = 6h$). (*a*) v_{rms}. (*b*) w_{rms}.

tensity is largest for SOF. The x-locations for the largest $w_{rms,max}$ shift upstream in control cases as compared to the uncontrolled case, indicating enhanced mixing at shorter downstream distances with controls.

Westphal, Johnston & Eaton (1984) reported that the reverse flow in the separation bubble is laminar-like but with high unsteadiness imposed by the turbulent shear layer. Le *et al.* (1997) also observed a similar trend in their DNS. They compared their DNS data with the empirical formula proposed by Adams, Johnston & Eaton (1984) for laminar C_f and suggested the following correlation from the computational

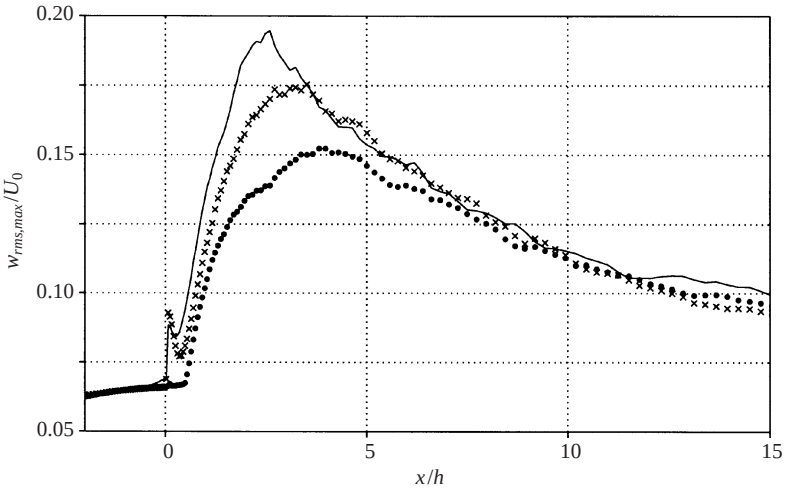

FIGURE 7. Maximum spanwise turbulence intensity along the streamwise direction: •, uncontrolled; ×, SFA ($St_h = 0.2$); ——, SOF ($x_s = 6h$).

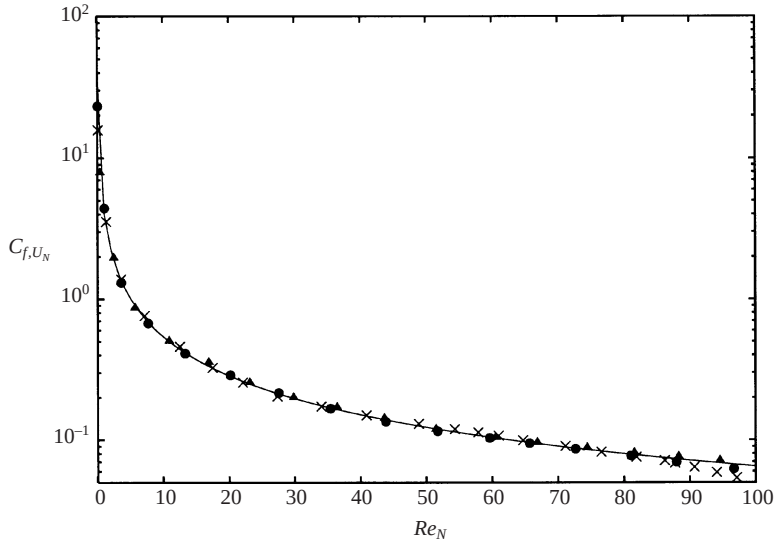

FIGURE 8. Friction coefficients in the separation bubble as a function of the wall-layer Reynolds number: ——, $C_{f,U_N} = 4.5Re_N^{-0.92}$; •, uncontrolled; ×, SFA ($St_h = 0.2$); ▲, SOF ($x_s = 6h$).

results,

$$C_{f,U_N} = 4.5Re_N^{-0.92}, \tag{4.2}$$

where $Re_N = U_N N/\nu$, U_N is the maximum negative mean velocity, N is the distance from the wall to the location of U_N, and C_{f,U_N} is the friction coefficient normalized by $\frac{1}{2}\rho U_N^2$. Figure 8 shows C_{f,U_N} obtained from the uncontrolled, SFA ($St_h = 0.2$) and SOF ($x_s = 6h$) cases, together with (4.2). An excellent agreement is observed in the overall range of Re_N for all the cases.

Figures 9(*a*) and 9(*b*) show the contours of the instantaneous spanwise and streamwise vorticity fluctuations, respectively. It is clear that both ω_x' and ω_z' are large even inside the recirculating bubble owing to control. Also, large ω_x' and ω_z' are observed

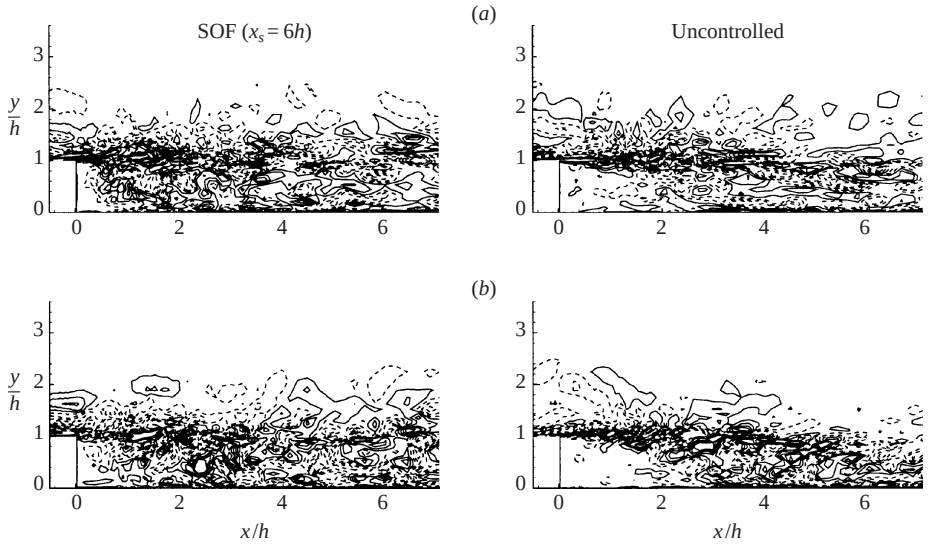

FIGURE 9. Contours of the instantaneous vorticity fluctuations in an (x, y)-plane: (a) $\omega_z' h/U_0$; (b) $\omega_x' h/U_0$. Contour levels are from -2.7 to 2.7 by increments of 0.6.

at $1 < y/h < 2$ in the downstream locations, as compared to the uncontrolled case. These are consistent with large v_{rms} and w_{rms} at those locations (figure 6).

4.3.2. *Actuation profile and mechanism*

It was shown in § 4.3.1 that SOF significantly increases mixing behind the backward-facing step. In this section, we present the actuation (blowing/suction) profile and the mechanism of mixing enhancement due to control.

Figure 10 shows the variation of the actuation profile due to different sensor locations. In this figure, the same instantaneous flow field is used to obtain the actuation profiles for different sensor locations. It is seen that the actuation profile is irregular in the spanwise direction when the sensor location ($x_s = 0$, $y_s = h$) is the same as the actuator location, but it becomes more sinusoidal as the sensor is located further downstream of the actuator location. The actuation profile in z at Γ_c is determined by the convolution integral of $\partial p'/\partial z$ and $\partial \pi'/\partial z$ at Γ_s as shown in (2.22). When the distance between the sensor and actuator becomes large, $\partial \pi'/\partial z \mid_{\Gamma_s}$ acts as a low-pass filter because π is determined by the Laplace equation with non-zero boundary condition at Γ_c (see (2.14)–(2.16)). Thus, only large-scale information of $\partial p'/\partial z \mid_{\Gamma_s}$ is delivered to the actuator location Γ_c, resulting in the sinusoidal profile of the actuation.

As is clear from figure 10, the actuation profile for $x_s = 6h$ and $y_s = 0$, which produced significant mixing enhancement, can be modelled as a sine function:

$$\phi(z, t) = A_0 \sin\left[\frac{2\pi}{L_z}(z + z_p(t))\right], \tag{4.3}$$

where the phase z_p is a function of time and is determined from the sensing of p_w' at $x_s = 6h$ and $y_s = 0$. Here, L_z is the domain size in the spanwise direction and is also the spanwise wavelength of the actuation. The effect of the actuation wavelength on mixing will be considered in § 4.4.

Figure 11 shows the time traces of the phase z_p in (4.3) for four different sensor lo-

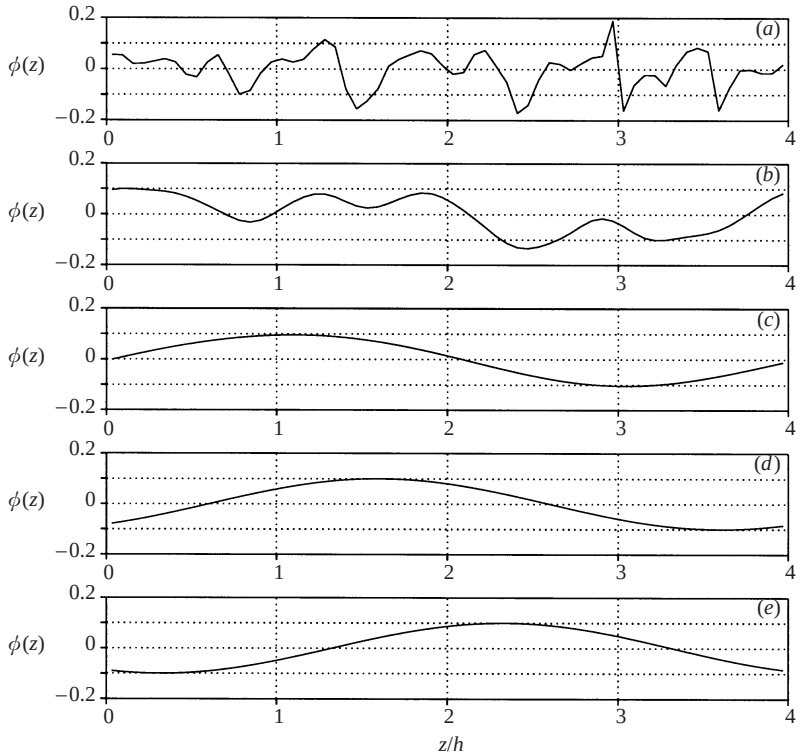

FIGURE 10. Variation of the actuation profile due to different sensor locations: (*a*) $x_s = 0$, $y_s = h$; (*b*) $x_s = 0$, $y_s = 0.8h$; (*c*) $x_s = y_s = 0$; (*d*) $x_s = 4h$, $y_s = 0$; (*e*) $x_s = 6h$, $y_s = 0$.

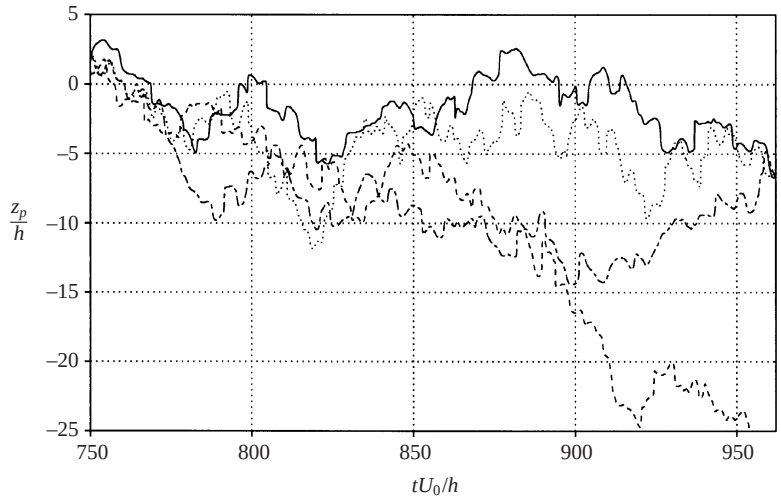

FIGURE 11. Time traces of the phase in (4.3): ——, $x_s = 4h$; – – –, $x_s = 5h$; · · ·, $x_s = 6h$; — · —, $5.5h < x_s < 6.5h$. Note that the spanwise domain length is $4h$ and thus the periodicity in z should be applied to $z_p > 4h$ and $z_p < 0$.

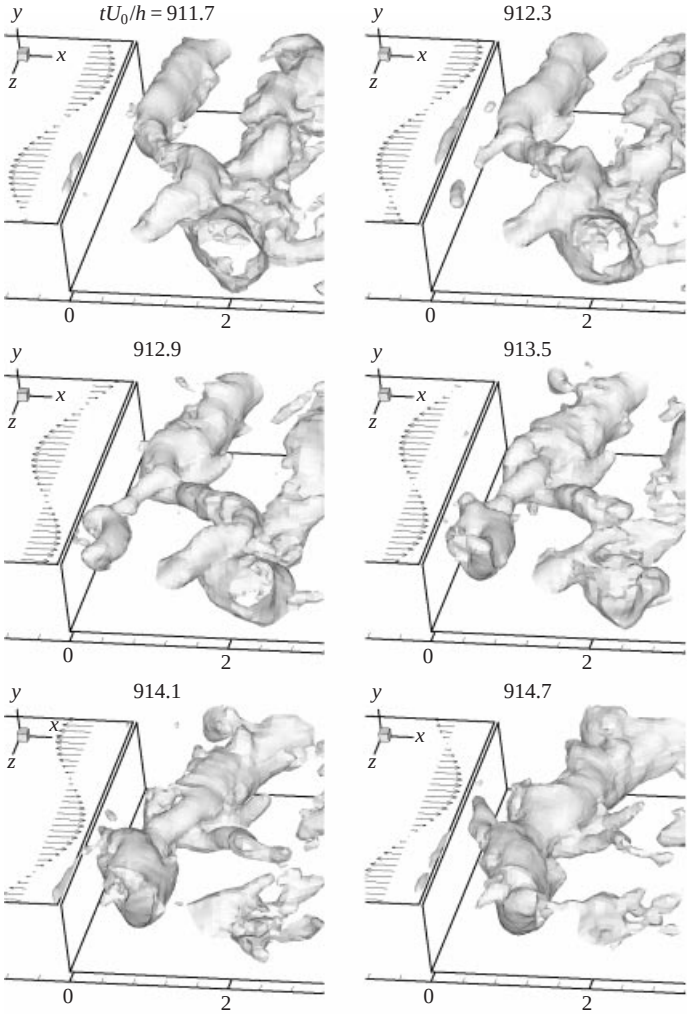

FIGURE 12. Time sequence of the pressure iso-surfaces ($p/\rho U_0^2 = -0.07$) for SOF ($x_s = 6h$). The vectors before the step denote the blowing/suction profile at each instance. Here, the arrow heading downstream denotes the blowing, and that heading upstream the suction.

cations. It is seen that the phase moves irregularly in time. It is worth investigating the effect of the phase movement on the vortex evolution behind the backward-facing step. It is well known from previous studies that the actuation with time-periodic blowing and suction generates roll-up vortices. Chun & Sung (1998) showed a clear visualization of this process. Also Mullin, Greated & Grant (1980) observed the occurrence of vortex shedding when the oscillating velocity is at its minimum. Figure 12 shows the time sequence of the pressure iso-surfaces for SOF, together with the blowing/suction profile at each instance. Each iso-surface of the low pressure is considered as a vortical structure (Robinson 1991). (We have also applied the vortex-identification method suggested by Jeong & Hussain (1995) and observed the same large-scale vortices as shown in figure 12, but with this method many small-scale vortices also appeared in the flow field.) It is clear that inclined vortical structures are generated near the step as the blowing/suction profile traverses in the spanwise direction. These inclined vortical structures have two components. One is the spanwise roll-up vortex which

is generated by local blowing and suction, and the other is the streamwise-vorticity component generated by tilting of the spanwise vorticity due to the phase movement in the spanwise direction. The irregular phase movement of the blowing/suction profile shown in figure 11 generates various sizes of inclined vortical structures. These vortical structures become closer owing to different convection velocities and interact among themselves in the downstream (figure 12). This vortical interaction increases mixing and reduces the reattachment length. The generation of inclined vortical structures and their spanwise deformation have been also observed in the experiment on a plane mixing layer where a time-harmonic excitation having spanwise-non-uniform phase or frequency distributions is imposed (see Nygaard & Glezer 1994).

As was shown in figure 10, the blowing/suction profile had small-scale variations in the spanwise direction when the distance between the sensor and actuator was small. When we applied actuations based on the sensing of p_w near the actuator location, the reattachment length was almost unchanged (the reason was given in § 4.3.1). We have also applied another suboptimal feedback control based on the sensing of p' at $x = 0.5h$ and $y = h$ (inside the domain). The blowing/suction profile also contained small-scale variations in this case. As a result, the turbulence intensities in the sensing region increased, but the overall increase in the turbulence intensity is not as much as that shown in figure 6 for SOF ($x_s = 6h$) and the reduction of the reattachment length was only half the maximum reduction shown in figure 4.

In order to investigate the possibility of small-scale forcing in increasing mixing, we applied an active feedback control developed by Choi, Moin & Kim (1994) to the present flow, in which the blowing/suction profile essentially had small-scale variations in space and time. The actuation increased the turbulence intensities at the actuator location, but did not change the reattachment length and the turbulence intensities behind the step (see Appendix A for details), indicating that the small-scale actuation alone does not significantly change the large-scale flow characteristics behind the step such as the recirculating bubble. In the case of SOF, when the distance between the sensor and actuator was sufficiently large, the actuation profile had mainly large-scale variations in the spanwise direction and in time (see figures 10 and 11). These combined large-scale variations in the actuation significantly increased mixing behind the backward-facing step.

4.4. *Open-loop controls*

As was shown in § 4.3.2, the blowing/suction profile from SOF could be modelled as (4.3), where $z_p(t)$ is determined by the sensing of p'_w at Γ_s (figure 11). In this section, we want to model $z_p(t)$ without any sensing. That is, we want to investigate the possibility of developing an open-loop (non-feedback) control method, which has nearly the same performance of mixing enhancement as that of the successful SOF, because, in general, open-loop control methods are much easier to implement in many physical systems than feedback control methods.

First, we test the following three phase functions:

$$z_p(t) = 0, \tag{4.4}$$

$$z_p(t) = 2h\mathrm{Rand}(t), \tag{4.5}$$

$$z_p(t) = V_p t, \tag{4.6}$$

where $\mathrm{Rand}(t)$ is a random function in t and V_p is a constant phase velocity. The first results in a stationary sinusoidal blowing/suction profile, introducing a spanwise inhomogeneous disturbance to the flow. The second has a Gaussian distribution of

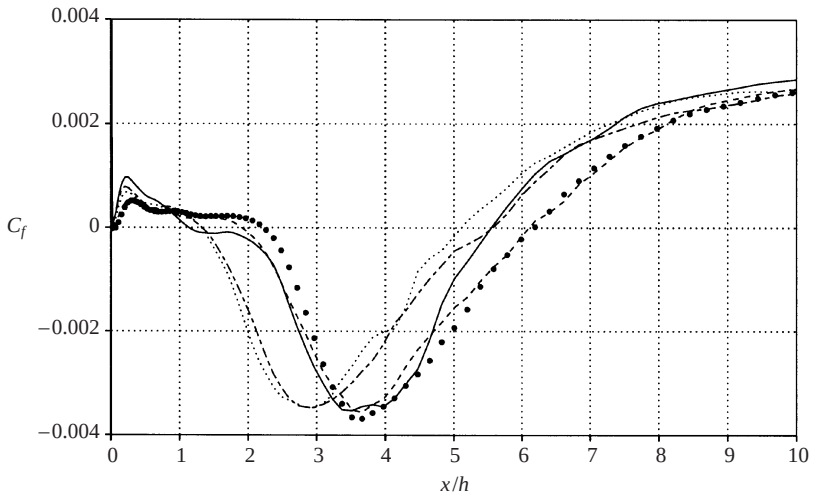

FIGURE 13. Variation of the friction coefficient due to different phase functions: •, uncontrolled; ——, $z_p(t) = 0$; – – –, $z_p(t) = 2h\text{Rand}(t)$; · · ·, $z_p(t) = 0.8U_0 \cdot t$; — · —, $z_p(t) = 1.2U_0 \cdot t$.

z_p from −2 to 2. This Gaussian distribution of z_p is introduced because the phase from SOF moves irregularly in time. The third has a sinusoidal profile moving at a constant velocity ($V_p/U_0 = 0.8$ and 1.2) in the spanwise direction. In the third case, the blowing/suction value at a fixed spanwise location is also sinusoidal in time because of the periodic boundary condition in the spanwise direction. The actuation frequencies corresponding to $V_p/U_0 = 0.8$ and 1.2 are $St_h = 0.2$ and 0.3, respectively. Therefore, the actuation with $z_p = V_p t$ has the characteristics of both the single-frequency actuation and actuation with (4.4).

Figure 13 shows the variation of the friction coefficient due to different phase functions. The stationary sine-wave actuation and sine-wave actuations moving in z at constant speeds reduce the reattachment length X_r, but the sine-wave actuation with random phases does not. The sine-wave actuation with $V_p/U_0 = 0.8$ results in more reduction in X_r than that with $V_p/U_0 = 1.2$, which makes sense because the former in part corresponds to the case of $St_h = 0.2$ and the latter to the case of $St_h = 0.3$. We showed in § 4.2 that the control at $St_h = 0.2$ reduces X_r more than that at $St_h = 0.3$. There may exist an optimal phase velocity for minimizing X_r, but further study was not performed here. However, all three phase functions tested ((4.4)–(4.6)) reduce the reattachment length by less than $1h$ (16.1%).

In figure 11, the phases from SOF looked irregular, but the actuation with purely random phases did not change the reattachment length. One important observation from figure 11 is that the phase z_p is still continuous (i.e. not perfectly random). Therefore, we suggest the following quasi-random phase (QRP) function for z_p:

$$z_p(t) = \alpha h \sum_i \text{Rand}_i(t), \tag{4.7}$$

where $\text{Rand}_i(t)$ ($-1 \leqslant \text{Rand}_i(t) \leqslant 1$) is generated at each computational time step, and α is the scaling parameter.

The open-loop control, (4.3) and (4.7), developed in this study (called QRP control hereinafter) has two parameters: the first is the spanwise wavelength for the actuation, L_z, and the second is the scaling parameter α.

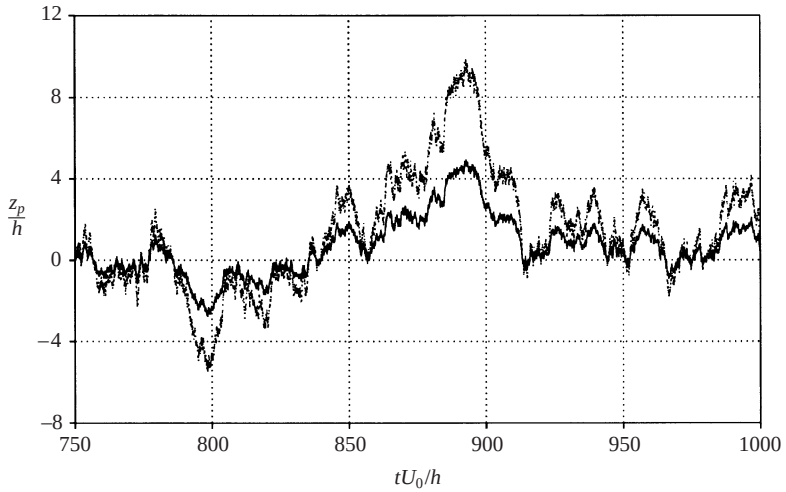

FIGURE 14. Examples of quasi-random phase: ——, $\alpha = 0.075$; · · ·, $\alpha = 0.15$. Note that the spanwise domain length is $4h$ and thus the periodicity in z should be applied to $z_p > 4h$ and $z_p < 0$.

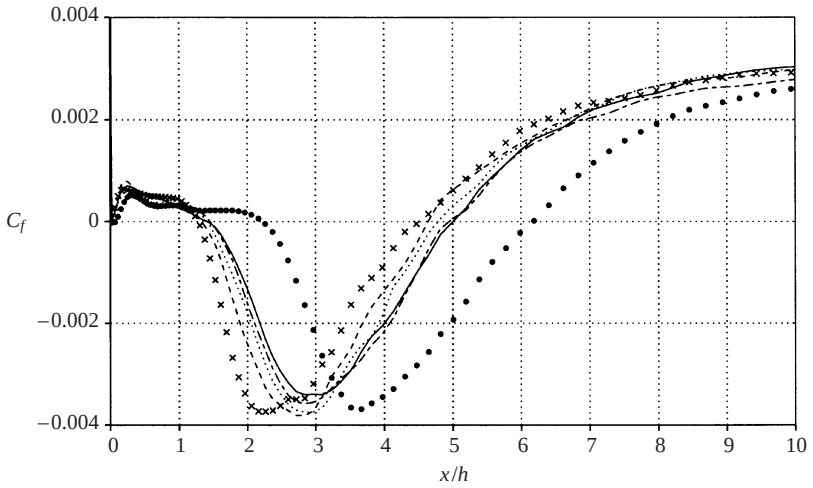

FIGURE 15. Friction coefficients: •, uncontrolled; ×, SOF ($x_s = 6h$); ——, QRP control with $\alpha = 0.075$; – – –, $\alpha = 0.15$; · · ·, $\alpha = 0.225$; — · —, $\alpha = 0.3$.

First, a parametric study is performed for the parameter α with $L_z = 4h$: $\alpha = 0.075$, 0.15, 0.225 and 0.3. Figure 14 shows the quasi-random phases generated at $\alpha = 0.075$ and 0.15. As shown in figure 14, increasing α increases the movement speed of the phase in the spanwise direction. Figure 15 shows the friction coefficients of four QRP controls, together with those of the uncontrolled and SOF cases. It is shown that the reduction of the reattachment length depends on α. The successful QRP control ($\alpha = 0.15$) reduces the reattachment length almost as much as the successful SOF does. The mechanism responsible for the reattachment-length reduction from QRP control is very similar to that from SOF, as shown in figure 12. A possible reason for the relatively poor performance with $\alpha = 0.075$ and 0.3 may be that too slow ($\alpha = 0.075$) or too fast ($\alpha = 0.3$) a phase velocity ($\mathrm{d}z_p/\mathrm{d}t$) is less effective in generating inclined large-scale structures found in figure 12.

So far, we have used $L_z = 4h$. Because the performance of QRP control in reducing

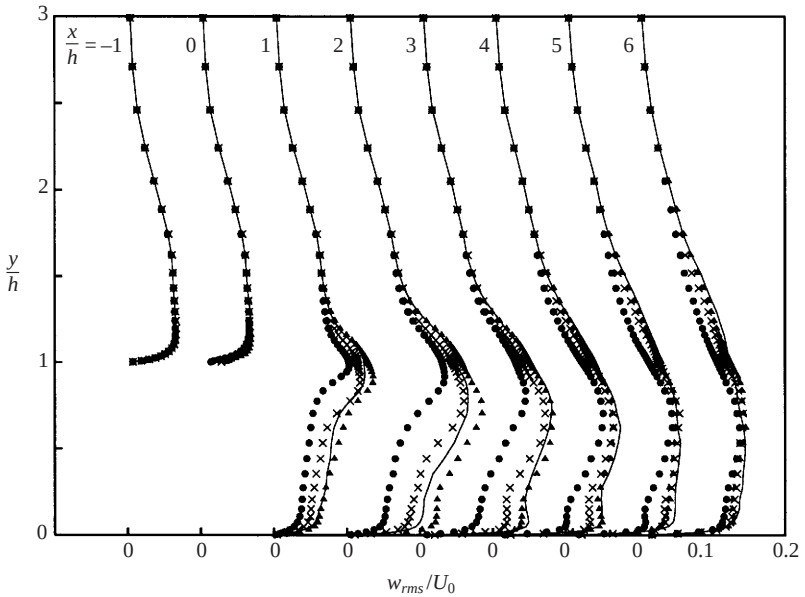

FIGURE 16. Root-mean-square spanwise velocity fluctuations: •, uncontrolled; ×, SFA ($St_h = 0.2$); ▲, SOF ($x_s = 6h$); ——, QRP control ($\alpha = 0.15$).

X_r depends also on L_z, we tried two more values of L_z, $2h$ and $8h$ with $\alpha = 0.15$. In the case of $L_z = 2h$, the reattachment length was about $5.4h$ (12.9% reduction), whereas it was about $4.9h$ (21.0% reduction) in the case of $L_z = 8h$. Therefore, the case with $L_z = 4h$ reduced the reattachment length most (27.4% reduction) among three different spanwise wavelengths.

Figure 16 shows the r.m.s. spanwise velocity fluctuations with and without controls. The r.m.s. spanwise velocity fluctuations significantly increase owing to the successful QRP control. The amount of increase in w_{rms} is nearly comparable to that of SOF. The same behaviour is also observed in u_{rms} and v_{rms} (not shown here).

5. Summary and concluding remarks

The objective of the present study was to increase mixing in turbulent flow behind a backward-facing step using a systematic feedback control method. Spatially and temporally varying blowing and suction with zero-net mass flow rate were provided from a slot located at the backward-facing step edge. To obtain a blowing/suction profile varying in the spanwise direction and time, the suboptimal feedback control procedure (Choi *et al.* 1993) was employed. The sensing variable was chosen to be the spanwise distribution of the wall-pressure fluctuations at a downstream location ($4h \sim 6.5h$ downstream of the step). The turbulent flow fields at $Re_h = U_0 h/\nu = 5100$ with and without controls were simulated using the LES technique, where U_0 is the free-stream velocity, h the step height, and ν the kinematic viscosity.

Prior to the suboptimal feedback control, time-periodic actuations were applied to turbulent flow over the backward-facing step. Among the cases with different actuation frequencies, the maximum reduction of the reattachment length, $1.2h$ (19.4%), was obtained at $St_h = fh/U_0 = 0.2$, where f is the actuation frequency. The suboptimal control procedure developed was applied to the same flow and its result was compared with that of the single-frequency actuation at $St_h = 0.2$. With the same r.m.s. value of

the actuation ($(0.1/\sqrt{2})U_0$), the suboptimal feedback control reduced the reattachment length more by the amount of $0.4h \sim 0.6h$ ($6.5\% \sim 9.7\%$) than the single-frequency actuation. The r.m.s. velocity and vorticity fluctuations significantly increased even inside the recirculating bubble owing to the suboptimal feedback control. Also, three-dimensional (inclined) large-scale vortical structures were generated behind the step by the control and their complex interactions occurred in the downstream. As a result, the cross-flow motions were very strong as compared to the uncontrolled and single-frequency actuation cases. All of these findings indicated enhanced mixing behind the backward-facing step owing to the suboptimal feedback control.

The actuation profile from the suboptimal feedback control was irregular in the spanwise direction when the sensor location was near the actuator location, but it became more sinusoidal as the sensor was located away from the actuator location. In the successful control cases, the distance between the sensor and actuator was large ($4h \sim 6.5h$) and thus the actuation profile was modelled as a sine function of the wavelength $4h$ in the spanwise direction with a temporally varying phase. In this case, the actuation profiles had large-scale variations in the spanwise direction and time. When the sensor was located near the actuator, the actuation profile was mainly composed of small-scale variations in the spanwise direction, which resulted in small or almost no changes in the reattachment length and turbulence intensities behind the step, indicating that the small-scale actuation alone does not significantly change the large-scale flow characteristics behind the step such as the recirculating bubble. The time sequence of the pressure iso-surfaces in the case of the successful suboptimal feedback control showed that inclined vortical structures are generated near the step as the blowing/suction profile traverses in the spanwise direction in time. The phase movement of the blowing/suction profile in time generated various sizes of inclined vortical structures and produced intensive vortical interactions, which significantly increased mixing behind the step. Therefore, the actuation with combined large-scale variations in the spanwise direction and in time was very effective in increasing mixing.

To develop a simple open-loop (non-feedback) control method from the result of the feedback control, we suggested a method of generating a quasi-random phase function. With a proper selection of the parameters in this function, the open-loop control increased mixing behind the step as much as the successful suboptimal feedback control did.

In the present study, we have paid special attention to the practical implementation of our control algorithm by placing sensors only at the wall (i.e. no measurement is required above the wall for the purpose of control). Nevertheless, the spatially and temporally varying actuation provides a certain difficulty in precisely implementing the control algorithm in a real situation; for example, temporally (quasi-randomly instead of periodically) varying blowing/suction signals are not so easy to realize accurately. Therefore, with a proper actuator developed for this purpose, the present numerical result should be validated by experiments in the future.

Financial support from the Creative Research Initiatives of the Korean Ministry of Science and Technology are gratefully acknowledged. We are also grateful to anonymous reviewers for their helpful comments on our paper.

Appendix A

To investigate the effect of small-scale forcing on the incoming turbulent boundary-layer flow on the downstream evolution of the backward-facing step flow, we apply

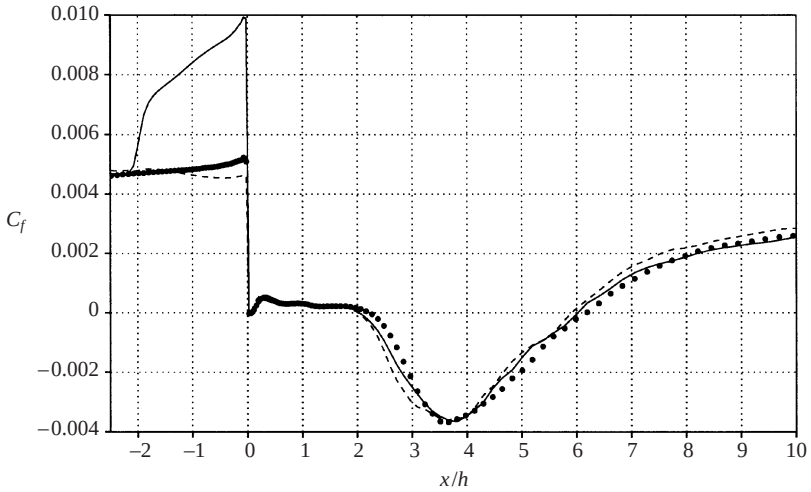

FIGURE 17. Friction coefficients: •, uncontrolled; ——, in-phase control; – – –, out-of-phase control.

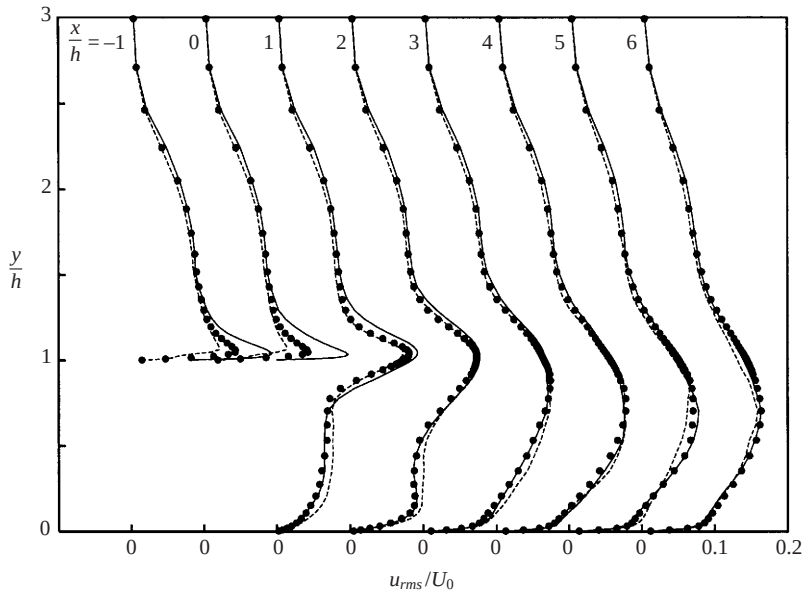

FIGURE 18. Root-mean-square streamwise velocity fluctuations: •, uncontrolled; ——, in-phase control; – – –, out-of-phase control.

a similar control strategy to that used in Choi *et al.* (1994). They showed that the near-wall streamwise vortices in a turbulent boundary layer can be intensified or weakened by providing blowing and suction at the wall, respectively, with the same (in-phase control) or opposite (out-of-phase control) value of the wall-normal velocity at $y^+ = 10$. Since the near-wall streamwise vortices are closely related with the near-wall turbulence intensity and mixing, manipulating them before the backward-facing step may have a significant effect on the flow downstream of the step.

In this study, we apply both the in-phase and out-of-phase controls to the incoming turbulent boundary-layer flow. The actuation region is selected to be $-2.5 \leqslant x/h \leqslant 0$

and $y = h$. Figure 17 shows the friction coefficients for the in-phase and out-of-phase control cases. As was shown in Choi *et al.* (1994), the skin-friction coefficient before the backward-facing step significantly increases with the in-phase control and decreases with the out-of-phase control. However, the reattachment length is not changed by these small-scale controls. A similar feature is also observed in the r.m.s. streamwise velocity fluctuations (figure 18), i.e. substantial changes are observed only before the step where the actuations are applied. A similar observation is also made for v_{rms} and w_{rms}. Therefore, it is concluded that when the incoming flow is a turbulent boundary-layer flow, small-scale forcing alone does not significantly change the flow behind the backward-facing step.

REFERENCES

Abergel, F. & Temam, R. 1990 On some control problems in fluid mechanics. *Theor. Comput. Fluid Dyn.* **1**, 303–325.

Adams, E. W., Johnston, J. P. & Eaton, J. K. 1984 Experiments on the structure of turbulent reattaching flow. *Rep.* MD-43. Department of Mechanical Engineering, Stanford University.

Akselvoll, K. & Moin, P. 1995 Large eddy simulation of turbulent confined coannular jets and turbulent flow over a backward facing step. *Rep.* TF-63. Department of Mechanical Engineering, Stanford University.

Bell, J. H. & Mehta, R. D. 1990 Development of a two-stream mixing layer from tripped and untripped boundary layers. *AIAA J.* **28**, 2034–2042.

Bell, J. H. & Mehta, R. D. 1993 Effects of imposed spanwise perturbations on plane mixing-layer structure. *J. Fluid Mech.* **257**, 33–63.

Bernal, L. P. & Roshko, A. 1986 Streamwise vortex structure in plane mixing layers. *J. Fluid Mech.* **170**, 499–525.

Bewley, T. R., Choi, H., Temam, R. & Moin, P. 1993 Optimal feedback control of turbulent channel flow. *Annu. Res. Briefs*, pp. 3–14. Center for Turbulence Research, Stanford University.

Bewley, T. R. & Moin, P. 1999 Optimal and robust control and estimation of transition, convection, and turbulence. *Rep.* TF-76. Department of Mechanical Engineering, Stanford University.

Bhattacharjee, S., Scheelke, B. & Troutt, T. R. 1986 Modification of vortex interactions in a reattaching separated flow. *AIAA J.* **24**, 623–629.

Breidenthal, R. 1981 Structure in turbulent mixing layers and wakes using a chemical reaction. *J. Fluid Mech.* **109**, 1–24.

Choi, H., Hinze, M. & Kunisch, K. 1999 Instantaneous control of backward-facing step flows. *Appl. Numer. Maths* **31**, 133–158.

Choi, H., Moin, P. & Kim, J. 1994 Active turbulence control for drag reduction in wall-bounded flows. *J. Fluid Mech.* **262**, 75–110.

Choi, H., Temam, R., Moin, P. & Kim, J. 1993 Feedback control for unsteady flow and its application to the stochastic Burgers equation. *J. Fluid Mech.* **253**, 509–543.

Chun, S., Lee, I. & Sung, H. J. 1999 Effect of spanwise-varying local forcing on turbulent separated flow over a backward-facing step. *Exps. Fluids* **26**, 437–440.

Chun, K. B. & Sung, H. J. 1996 Control of turbulent separated flow over a backward-facing step by local forcing. *Exps. Fluids* **21**, 417–426.

Chun, K. B. & Sung, H. J. 1998 Visualization of a locally-forced separated flow over a backward-facing step. *Exps. Fluids* **25**, 133–142.

Collis, S. S., Lele, S. K., Moser, R. D. & Rogers, M. M. 1994 The evolution of a plane mixing layer with spanwise nonuniform forcing. *Phys. Fluids* **6**, 381–396.

Eaton, J. K. & Johnston, J. P. 1980 Turbulent flow reattachment: an experimental study of the flow and structure behind a backward-facing step. *Rep.* MD-39. Department of Mechanical Engineering, Stanford University.

Eaton, J. K. & Johnston, J. P. 1981 A review of research on subsonic turbulent flow reattachment. *AIAA J.* **19**, 1093–1100.

Fessler, J. R. & Eaton, J. K. 1999 Turbulence modification by particles in a backward-facing step flow. *J. Fluid Mech.* **394**, 97–117.

Finlayson, B. A. 1972 *The Method of Weighted Residuals and Variational Principles*. Academic.

Germano, M., Piomelli, U., Moin, P. & Cabot, W. H. 1991 A dynamic subgrid-scale eddy viscosity model. *Phys. Fluids* A **3**, 1760–1765.

Glowinski, R. & Pironneau, O. 1992 Finite element methods for Navier–Stokes equations. *Annu. Rev. Fluid Mech.* **24**, 167–204.

Hasan, M. A. Z. & Khan, A. S. 1992 On the instability characteristics of a reattaching shear layer with nonlaminar separation. *Intl J. Heat Fluid Flow* **13**, 224–231.

Heenan, A. F. & Morrison, J. F. 1998 Passive control of pressure fluctuations generated by separated flow. *AIAA J.* **36**, 1014–1022.

Hou, L. S. & Ravindran, S. S. 1998 Penalty methods for numerical approximations of optimal boundary flow control problems. *Intl J. Comput. Fluid Dyn.* **11**, 157–167.

Hou, L. S. & Ravindran, S. S. 1999 Numerical approximation of optimal flow control problems by a penalty method: error estimates and numerical results. *SIAM J. Sci. Comput.* **20**, 1753–1777.

Isomoto, K. & Honami, S. 1989 The effect of inlet turbulence intensity on the reattachment process over a backward-facing step. *Trans. ASME: J. Fluids Engng* **111**, 87–92.

Jeong, J. & Hussain, F. 1995 On the identification of a vortex. *J. Fluid Mech.* **285**, 69–94.

Jovic, S. & Driver, D. M. 1994 Backward-facing step measurement at low Reynolds number, $Re_h = 5000$. *NASA Tech. Mem.* 108807.

Karasso, P. S. & Mungal, M. G. 1997 Mixing and reaction in curved liquid shear layers. *J. Fluid Mech.* **334**, 381–409.

Kim, B. N. & Chung, M. K. 1995 Experimental study of roughness effects on the separated flow over a backward-facing step. *AIAA J.* **33**, 159–161.

Kim, J. & Moin, P. 1985 Application of a fractional-step method to incompressible Navier–Stokes equations. *J. Comput. Phys.* **59**, 308–323.

Lasheras, J. C., Cho, J. S. & Maxworthy, T. 1986 On the origin and evolution of streamwise vortical structures in a plane, free shear layer. *J. Fluid Mech.* **172**, 231–258.

Le, H., Moin, P. & Kim, J. 1997 Direct numerical simulation of turbulent flow over a backward-facing step. *J. Fluid Mech.* **330**, 349–374.

Lee, C., Kim, J. & Choi, H. 1998 Suboptimal control of turbulent channel flow for drag reduction. *J. Fluid Mech.* **358**, 245–258.

Lee, S., Lele, S. K. & Moin, P. 1992 Simulation of spatially evolving turbulence and the applicability of Taylor's hypothesis in compressible flow. *Phys. Fluids* A **4**, 1521–1530.

Lilly, D. K. 1992 A proposed modification of the Germano subgrid-scale closure method. *Phys. Fluids* A **4**, 633–635.

Lund, T. S., Wu, X. & Squires, K. D. 1998 Generation of turbulent inflow data for spatially-developing boundary layer simulations. *J. Comput. Phys.* **140**, 233–258.

Min, C. & Choi, H. 1999 Suboptimal feedback control of vortex shedding at low Reynolds numbers. *J. Fluid Mech.* **401**, 123–156.

Mullin, T., Greated, C. A. & Grant, I. 1980 Pulsating flow over a step. *Phys. Fluids* **23**, 669–674.

Nygaard, K. J. & Glezer, A. 1994 The effect of phase variations and cross-shear on vortical structures in a plane mixing layer. *J. Fluid Mech.* **276**, 21–59.

Pauley, L. L., Moin, P. & Reynolds, W. C. 1990 The structure of two-dimensional separation. *J. Fluid Mech.* **220**, 397–411.

Pumir, A. 1994 A numerical study of the mixing of a passive scalar in 3 dimensions in the presence of a mean gradient. *Phys. Fluids* **6**, 2118–2132.

Robinson S. K. 1991 The kinematics of turbulent boundary layer structure. *NASA Tech. Mem.* 103859.

Roos, F. W. & Kegelman, J. T. 1986 Control of coherent structures in reattaching laminar and turbulent shear layers. *AIAA J.* **24**, 1956–1963.

Satake, S. & Kasagi, N. 1997 Suboptimal turbulence control with the body force of selective velocity damping localized to the near-wall region. *Proc. 11th Symp. Turbulent Shear Flows, Grenoble, September 1997*, vol. 1, pp. P1.43–P1.48.

Selby, G. V., Lin, J. C. & Howard, F. G. 1990 Turbulent flow separation control over a backward-facing ramp via transverse and swept grooves. *Trans. ASME: J. Fluids Engng* **112**, 238–240.

Sigurdson, L. W. 1995 The structure and control of a turbulent reattaching flow. *J. Fluid Mech.* **298**, 139–165.

WESTPHAL, R. V., JOHNSTON, J. P. & EATON, J. K. 1984 Experimental study of flow reattachment in a single-sided sudden expansion. *Rep.* MD-41. Department of Mechanical Engineering, Stanford University.

YANG, J. T., TSAI, B. B. & TSAI, G. L. 1994 Separated-reattaching flow over a backstep with uniform normal mass bleed. *J. Fluids Engng* **116**, 29–35.